EUROPEAN LABORATORY FOR PARTICLE PHYSICS (CERN)

ICHEP 2000
Abstract **304**
Parallel Sessions **05a**
Plenary Sessions **06a**

ALEPH/2000-054
CONF/2000-036
July 13, 2000

PRELIMINARY

Single W Production at Energies up to $\sqrt{s} = 202\,\mathrm{GeV}$ and Search for Anomalous Triple Gauge Boson Couplings

The ALEPH Collaboration

Contact person: Vincent Lemaitre *(Vincent.Lemaitre@cern.ch)*

Abstract

The four fermion process $e^+e^- \to e\nu f\bar{f}'$, compatible with a single W production, has been studied using the data recorded with the ALEPH detector at centre-of-mass energies between 161 and 202 GeV, corresponding to an integrated luminosity of 490 pb^{-1}. The cross sections for single W production have been measured and are in good agreement with the Standard Model expectations. The average ratio between the measured single W cross sections and the standard model expectations is found to be $0.87 \pm 0.13(stat.) \pm 0.09(syst.) \pm 0.05(theory)$. The 95% confidence level limits on anomalous triple gauge couplings are found to be $-0.54 < \Delta\kappa_\gamma < 0.15(\lambda_\gamma = 0)$ and $-0.57 < \lambda_\gamma < 0.44(\Delta\kappa_\gamma = 0)$.

(ALEPH contribution to 2000 summer conferences)

1 Introduction

The study of $e^+e^- \rightarrow e\nu$W at LEP2 is an interesting investigation of possible physics beyond the Standard Model. In particular, it probes the $SU(2)_L \times U(1)_Y$ gauge group structure of the theory via its strong sensitivity to WWγ triple gauge couplings [1].

ALEPH has studied single W production at LEP2 at energies up to 202 GeV [2, 3, 4] where a measurement of the single W cross section up to 202 GeV, limits on anomalous Triple Gauge Couplings (TGC) for energies up to 189 GeV and a search for monojet events have been presented.

This note presents new limits on TGCs using data collected at centre-of-mass energies between 183 and 202 GeV, corresponding to an integrated luminosity of 490 pb^{-1}. The measurement of single W cross sections presented in [4] is also summarised in this note for the sake of completeness.

The note is organised as follows. The reconstruction, the selection and the simulation of events is presented in section 2, the treatment of systematic uncertainties is given in section 3 and the measurement of single W cross sections is summarised in section 4. Section 5 briefly describes the method to extract anomalous couplings and the results are presented in section 6, followed by the conclusion in section 7.

2 Reconstruction, Selection and Simulation of Events

2.1 Event Reconstruction

This study is based on data recorded with the ALEPH detector at centre-of-mass energies of 161.3, 172.1, 182.7, 188.6, 191.6, 195.5, 199.5 and 201.6 GeV with integrated luminosities of 11.1, 10.8, 57, 174.2, 28.92, 79.83, 86.30 and 41.98 pb^{-1},respectively.

A detailed description of the ALEPH detector can be found in [5]. Here, only the relevant parts are briefly described. The tracking system consists of a silicon vertex detector (VDET), a drift chamber (ITC) and a large time projection chamber (TPC), all situated in a 1.5 Tesla magnetic field provided by a superconducting solenoidal coil. In this analysis, a good track is defined as having at least four TPC hits and a value of $|cos(\theta)| < 0.98$. Moreover it must originate within a cylinder of 10cm length and 2cm radius centred at the nominal interaction point and parallel to the beam. Particle identification is performed using information mainly from the TPC (dE/dx, γ conversion, V_0 finding), the electromagnetic calorimeter (ECAL), the hadronic calorimeter (HCAL) and large muon chambers surrounding the HCAL. The particle identification and the kinematical information from these detectors are combined in an energy flow algorithm [6]. For each event, the algorithm provides a set of charged and neutral reconstructed particles which are used in the analysis.

The dominant diagrams for single W production are shown in Fig. 1 for the $e^-\bar{\nu}_e u\bar{d}$ (CC20) final state. The first $\gamma -$ W fusion diagram is sensitive to the WWγ coupling. The photon exchanged in these diagrams is quasi-real, thus the outgoing electron is predominantly emitted at small polar angles. Another specific feature is the large missing momentum carried away by the electron-neutrino.

All W decay modes are analysed. Leptonic W decays are characterised by a high

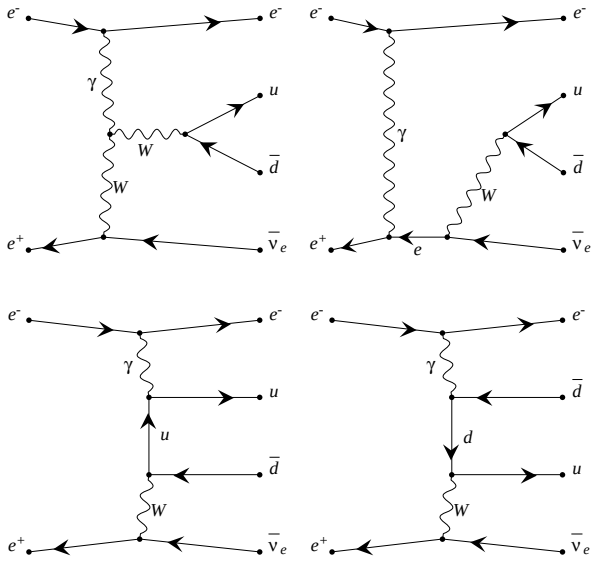

Figure 1: Dominant t-channel diagrams for the process of $e^+e^- \to e^-\bar{\nu}_e u\bar{d}$; from top left to bottom right: $\gamma - \mathrm{W}$ fusion, W-bremsstrahlung, and two multi-peripheral diagrams.

energy isolated lepton. Hadronic W decays are characterised by two acoplanar jets with an invariant mass around that of the W boson.

The present selection is optimised for the definition of the single W cross section used in previous ALEPH analyses [2, 3]:

$$\begin{cases} \theta_{\mathrm{e}} < 34\,\mathrm{mrad}, & \\ \mathrm{E}_\ell > 20\,\mathrm{GeV} \text{ and } |\cos\theta_\ell| < 0.95 & \text{for the leptonic decay,} \\ \mathrm{M}_{\mathrm{q\bar{q}'}} > 60\,\mathrm{GeV}/c^2 & \text{for the hadronic decay,} \end{cases} \tag{1}$$

where θ_{e} is the polar angle of the scattered electron, E_ℓ and θ_ℓ are the energy and polar angle of leptons from the W decay. $\mathrm{M}_{\mathrm{q\bar{q}'}}$ is the invariant mass of the quark pair. The cut angle at 34 mrad corresponds to the lower edge of the acceptance of the ALEPH detector.

2.2 Leptonic Selection

The selection cuts are almost the same as in the analysis at $\sqrt{s} = 183\,\mathrm{GeV}$ [2] and are summarised here.

For leptonic decays of the W boson, a single track is expected for the electron, muon or single prong tau decay. A higher multiplicity is expected for other tau decays. Therefore events with one or three good charged tracks are accepted. Moreover, events with at least one bad charged track are rejected.

The polar angle of the missing momentum direction θ_{miss} is required to satisfy $|\cos\theta_{\mathrm{miss}}| < 0.9$. Tagged two-photon events are rejected by requiring that no energy be detected within a cone of 12° around the beam axis (E_{12}).

The remaining backgrounds, mainly untagged two-photon events and two-fermion events, are eliminated by requiring that the transverse missing momentum be greater than $0.06\sqrt{s}$. This threshold is increased to $0.10\sqrt{s}$ if the missing momentum direction

points to within 10° in azimuth to the boundaries between the two LCAL halves or the six inner sectors of the TPC. It is required that no energy is found within a ϕ-wedge of 10° opposite to the direction of the charged transverse momentum. To reduce the background from the Zee process with Z decaying to neutrinos, events are rejected if an electron is identified and its energy is less than 20 GeV. The background from the $\nu\nu\gamma$ process where the photon undergoes asymmetric conversion and is identified as an electron, is strongly reduced by requiring at least one coordinate in the vertex detector (the latter cut is not applied to the 183 GeV data).

The typical efficiencies for the leptonic decay modes at centre-of-mass energies between 189 and 202 GeV are 74% (electron), 76% (muon) and 40% (tau), respectively, and are slightly better at 183 GeV. The main background source is the Zee process where Z decays to $\nu_\mu\bar{\nu_\mu}$ or $\nu_\tau\bar{\nu_\tau}$ (the $\nu_{\mathrm{e}}\bar{\nu_{\mathrm{e}}}$ case is a four-fermion final state which is eνW-like and is part of the signal).

In the data, a total of 54 events are observed in reasonable agreement with the expectation from the Standard Model of 70.4 events (51.1 signal events). The composition is 34 events with an electron, 9 events with a muon and 11 events with a tau.

2.3 Hadronic Selection

2.3.1 Pre-selection cuts

For hadronic decays of the W boson a Neural Network especially trained to reduce the WW and the ZZ backgrounds is used. The pre-selection criteria are defined from a subset of cuts used (and optimised) for the selection of events at $\sqrt{s} = 183$ GeV [2] (the selection of events at 183 GeV has not been changed).

First, a control sample of events is defined where most of tagged two-photon events and two-fermion events with initial state radiation are rejected. At least seven good charged tracks are required, the polar angle of the missing momentum direction is required to satisfy $|\cos\theta_{\mathrm{miss}}| < 0.9$. The acollinearity angle between the two hemisphere momentum directions is required to be less than 165°, and events for which the energy in a ϕ-wedge of 30° centred on the transverse missing momentum direction is greater than $0.20\sqrt{s}$ are rejected. Untagged two-photon events are rejected by requiring that the visible mass exceed 40 GeV/c^2.

A pre-selection is then defined before the training of the Neural Network in such a way that the background sources other than WW and ZZ are further reduced. Tagged two-photon events and two-fermion events with initial state radiation are rejected by demanding that the energy E_{12} be less than $0.025\sqrt{s}$. Events for which the energy in a ϕ-wedge of 30° centred on the transverse missing momentum direction is greater than $0.10\sqrt{s}$ are rejected. Since the ALEPH definition of the cross section requires the invariant mass of the quark pair to be above 60 GeV/c^2, a visible mass exceeding 60 GeV/c^2 is required.

In addition, the semileptonic ($l\nu\mathrm{q}\bar{\mathrm{q}}'$) W pair events are efficiently rejected by requiring that no identified electron or muon with an energy of more than $0.05\sqrt{s}$ be reconstructed.

After this pre-selection, the remaining events originate mainly from the eνW, ZZ and WW processes. The main contribution comes from W pairs where one of the W decays into $\tau\nu$ and the tau decays hadronically. This is illustrated in Fig. 2 showing the

distributions of events passing the pre-selection as a function of the visible invariant mass.

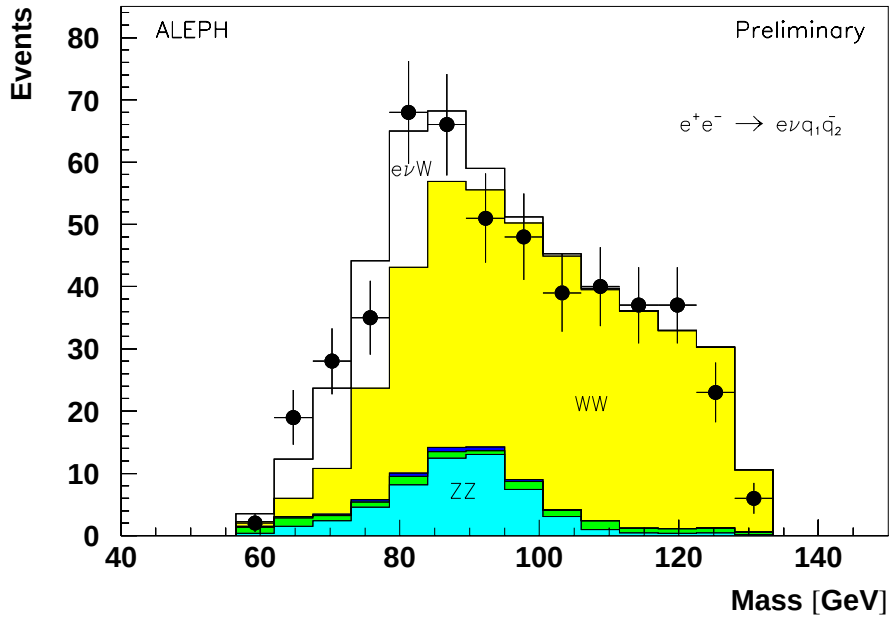

Figure 2: Comparison between distributions from the simulation (histogram) and the data (point) for the pre-selected sample of $189-202$ GeV data, as function of the visible invariant mass. The displayed histograms represent from top to bottom the eνW, WW, various other processes, q$\bar{\text{q}}$ and ZZ contributions, respectively. At this stage, the q$\bar{\text{q}}$ and various other processes are almost completely rejected.

2.3.2 Neural Network selection

A neural network analysis is applied to the sample of events surviving the pre-selection cuts defined in the previous section. Two sets of variables are used. The first set consists of the following global variables: the thrust, the sphericity, the acoplanarity, $\mathrm{E_{vis}}/\sqrt{s}$, $\mathrm{M_{vis}}/\mathrm{E_{vis}}$ and $\mathrm{P_{t_{miss}}}/\mathrm{E_{vis}}$, where $\mathrm{E_{vis}}$, $\mathrm{M_{vis}}$ and $\mathrm{P_{t_{miss}}}$ are the visible energy, mass and missing transverse momentum.

In addition to the six global variables, a tau-jet reconstruction algorithm is used and an event is classified as having a tau if the charged momentum of the tau candidate is above $0.025\sqrt{s}$. For those events, four additional variables are used as input to the Neural Network. They are $\mathrm{P_{ch}}/\mathrm{E_{vis}}$, $\mathrm{E}_\tau/\mathrm{E_{vis}}$,$M_{ww}/\mathrm{E_{vis}}$ and $Acol_{ww}$, where $\mathrm{P_{ch}}$ and E_τ are the charged momentum and the energy of the tau candidate and M_{ww} and $Acol_{ww}$, the visible invariant mass and the acollinearity, calculated excluding the tau object.

The training of the Neural Network is done using the MLPFIT package interfaced with PAW [7]. The distribution of the output neuron is shown in Fig. 3 for $189-202$ GeV data. The value of the cut (0.65) of the Neural Network output is chosen to maximise the product of efficiency and purity. Above this cut, a clear signal is observed.

The efficiency at $189-202$ GeV (calculated using the ALEPH definition of the cross section) for the hadronic decays of the W is about 50%. In the data, including 183 GeV

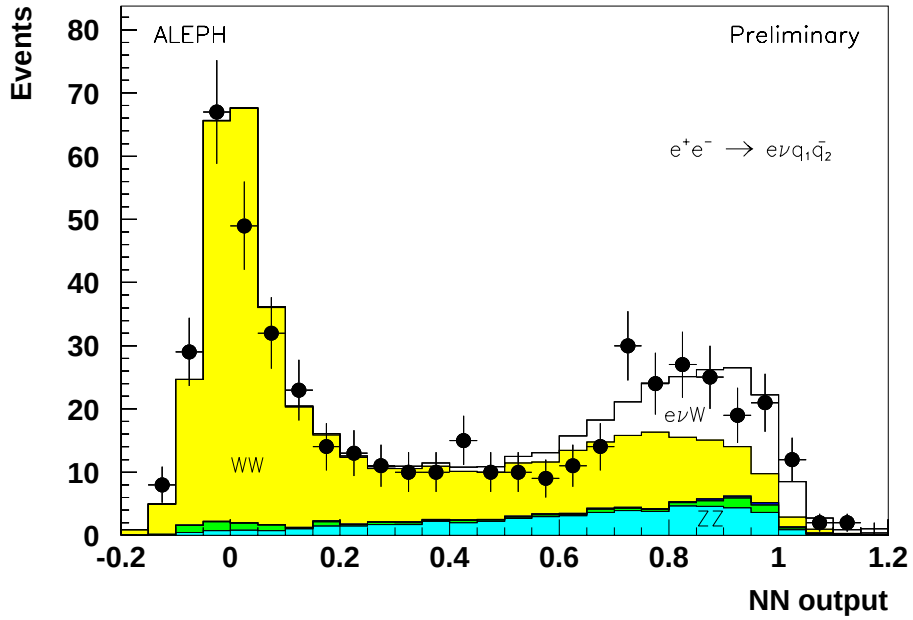

Figure 3: Comparison between distributions from the simulation (histogram) and the data (point) for the pre-selected sample of $189 - 202\,\text{GeV}$ data for the neural network output. A cut at 0.65 together with the pre-selection cuts defines the selected sample. The displayed histograms represent from top to bottom the eνW, WW, various other processes, $q\bar{q}$ and ZZ contributions, respectively. At this stage, the $q\bar{q}$ and various other processes are almost completely rejected

data, 193 events are observed, in agreement with the Standard Model expectation of 193.2 events (77.4 signal events). A single W candidate event at 200 GeV is shown in Fig. 4.

2.4 Monte Carlo Samples

The GRC4F program [8] is used to simulate the four-fermion final state $e\nu f\bar{f}'$ in order to study single W production. Final state radiation is simulated with the PHOTOS [9] package. Tau decays are generated with TAUOLA [10].

Two fermion processes are generated with UNIBAB(e^+e^-) [11] and KORALZ($q\bar{q}$, $\mu^+\mu^-, \tau^+\tau^-, \nu\bar{\nu}(\gamma)$) [12] (PYTHIA [13] is used for $q\bar{q}$ process at $183 - 189\,\text{GeV}$). W pair production is simulated with KORALW [14]. PYTHIA is used to generate other four-fermion processes such as ZZ and Zee. Finally, PHOT02 [15] and PYTHIA are used to simulate two photon processes.

3 Systematic uncertainties

Different sources of systematic errors can affect the measurement of the leptonic and the hadronic cross sections.

- Theoretical errors: the uncertainty on the normalisation of the various background sources is taken to be $\pm 2\%$ for WW, ZZ and Z$\nu\nu$ processes, $\pm 20\%$ for Zee process,

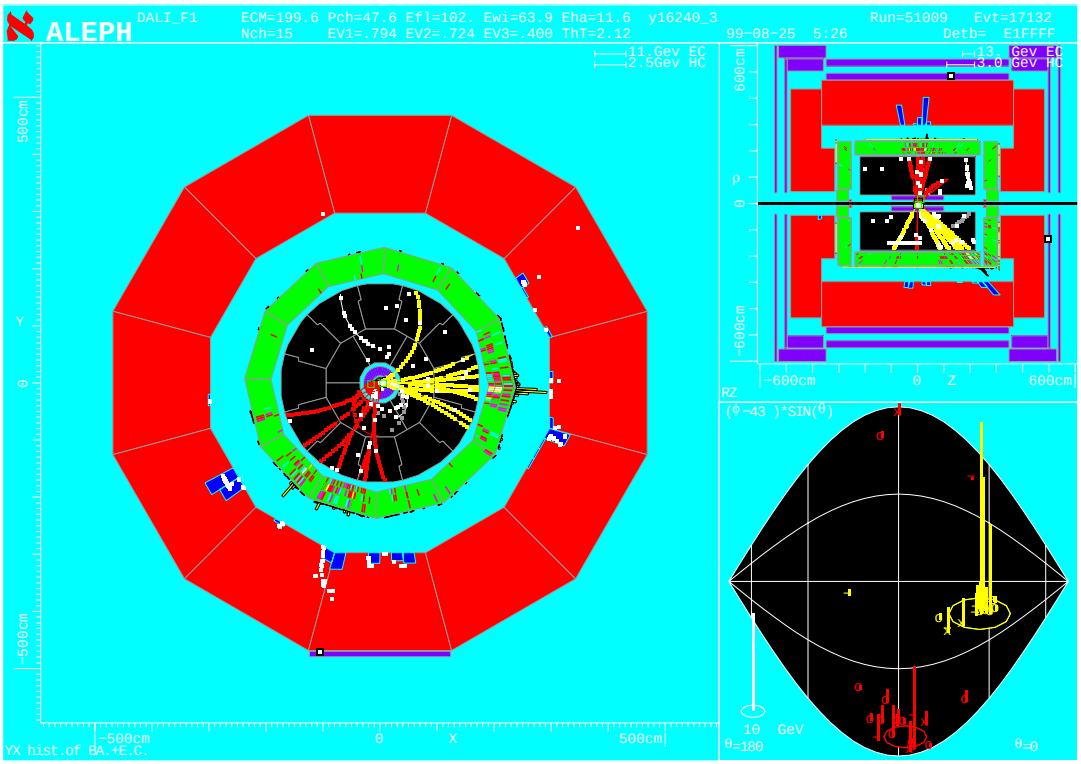

Figure 4: Event candidate of single W decaying into hadrons produced at 200 GeV.

$\pm 5\%$ for the two fermion final states generated with PYTHIA and $\pm 30\%$ on $\gamma\gamma$ processes.

- Experimental errors: the uncertainty on the integrated luminosity is estimated to be $\pm 0.7\%$. The uncertainty on the absolute energy scale of the electromagnetic and the hadronic calorimeters is $\pm 0.9\%$ and $\pm 2\%$, respectively [6]. Effects from possible tracking distortions have been assessed by applying or not applying the correction factors determined using $Z \to \mu^+\mu^-$ events collected in calibration runs at the Z peak. Pending further studies, the error on the single muon efficiency was set to 4% and the uncertainties on the jet energy correction, the LEP energy and the fragmentation models have been neglected.

Systematic uncertainties of the cut analysis have been studied in detail for 189 GeV data and are summarised in table 1 for the leptonic and the hadronic cross sections.

Source	$\Delta\sigma_{lep}/\sigma_{lep}$	$\Delta\sigma_{had}/\sigma_{had}$
Luminosity	± 0.011	± 0.029
Absolute Energy Scale	± 0.001	$^{+0.110}_{-0.079}$
Tracking	± 0.000	± 0.000
Trigger	± 0.014	± 0.000
Theory (MC)	± 0.062	± 0.049
quadratic mean	± 0.065	$^{+0.12}_{-0.10}$

Table 1: Summary of the systematic uncertainties for the leptonic and the hadronic cross sections

A systematic error of about 7% for the leptonic and 11% for the hadronic channels is observed. The main contribution comes from the uncertainty in the absolute energy scale of the calorimeters. In order to estimate the uncertainties for the new hadronic selection, it was checked that the same relative error coming from this source was obtained.

For these preliminary results, the experimental systematic errors at energies above 189 GeV are obtained assuming that the relative systematic error be similar to the one calculated at 189 GeV.

Finally, the stability of the cut analysis (which constitutes essentially the pre-selection for the hadronic channel) with respect to the event selection is tested by varying the main selection within reasonable limits; no significant shift is observed.

In order to determine the systematic error on the couplings, it is assumed (conservatively) that the main sensitivity comes from the hadronic decay, and that the uncertainty on the couplings will entirely come from the systematic uncertainty on the measured hadronic single W cross section. Therefore, a 12% uncertainty is applied on the $e\nu$W process from which a new χ^2 is obtained.

4 Measurement of Single W Cross sections

Recently, the four LEP experiments have agreed upon a common definition for the single W cross section in order to ease the combination of the results. The choice of the definition

is driven by the necessity to enhance the diagrams where the W can be on-shell while keeping the calculation gauge invariant:

$$\begin{cases} ee\nu\nu: & t-ch \text{ diag.} \quad \mathrm{E}_{e^+} > 20\,\mathrm{GeV} \text{ and } |\cos\theta_{e^+}| < 0.95, |\cos\theta_{e^-}| > 0.95 (\text{and cc}) \\ e\nu\ell\nu: & t-ch \text{ diag.} \quad \mathrm{E}_{\ell} > 20\,\mathrm{GeV} (\ell = \mu, \tau) \\ e\nu qq': & t-ch \text{ diag.} \quad \mathrm{M}_{q\bar{q}'} > 45\,\mathrm{GeV}/c^2. \end{cases} \tag{2}$$

An effective QED coupling constant is used in the calculation and is defined as $\alpha^4 = \alpha^2(0) * \alpha^2(\mathrm{M}_\mathrm{W}^2) = (1/132.44)^4$, where the exchanged photon is assumed to be quasi-real or rescaled at M_W^2 if linked to a W-vertex.

The cross section resulting from this definition is about 1.5 times larger than the one calculated with the ALEPH definition. The overall theoretical uncertainty on the prediction calculated with GRC4F is assumed to be 5%.

To determine the cross section, the Standard Model W branching ratios are assumed. First, the cross section is determined according to the ALEPH definition, then a correction factor is applied to obtain the LEP definition.

Preliminary ALEPH measurements of the leptonic, hadronic and total cross sections are shown respectively in table 2, 3 and 4 for six different centre-of-mass energies. The first error assigned to the measured cross section is the statistical error and the second is the systematic error. These systematic errors also include the uncertainties due to the limited Monte Carlo statistics.

Results at 183 GeV are obtained by a rescaling the results from a previous analysis [2].

CM energy[GeV]	σ_{lep} [pb]	σ_{lep}(GRC4F) [pb]	Ratio
182.7	$0.21 \pm 0.10 \pm 0.02$	0.206 ± 0.010	1.02 ± 0.49
188.6	$0.14 \pm 0.06 \pm 0.01$	0.230 ± 0.012	0.61 ± 0.26
191.6	$0.37 \pm 0.19 \pm 0.03$	0.242 ± 0.012	1.53 ± 0.79
195.5	$0.20 \pm 0.09 \pm 0.02$	0.259 ± 0.013	0.77 ± 0.35
199.5	$0.18 \pm 0.09 \pm 0.02$	0.276 ± 0.014	0.65 ± 0.33
201.6	$0.07 \pm 0.10 \pm 0.01$	0.285 ± 0.014	0.25 ± 0.35

Table 2: Measured and predicted leptonic cross sections for different centre-of-mass energies and the ratios between experiment and theory. For the ratios, only statistical errors are shown.

A good agreement is observed between these measurements and the Standard Model calculation of GRC4F, also shown in these tables. The total cross section is shown in Fig. 5. On these figures, only statistical errors are shown and a relative theoretical uncertainty of 5% is assumed.

5 Measurement of Triple Gauge Boson Couplings

In this analysis, the anomalous couplings are extracted by performing a generalised unbinned maximum log-likelihood fit by maximising the log-likelihood function,

$$\log L = N \log N_\sigma(\bar{\alpha}) - N_\sigma(\bar{\alpha}) + \Sigma_{i=1}^{N} \log P(O_i, \bar{\alpha}), \tag{3}$$

CM energy[GeV]	σ_{had} $[pb]$	σ_{had}(GRC4F) $[pb]$	Ratio
182.7	$0.40 \pm 0.23 \pm 0.06$	0.419 ± 0.021	0.95 ± 0.55
188.6	$0.31 \pm 0.13 \pm 0.04$	0.470 ± 0.024	0.66 ± 0.28
191.6	$0.94 \pm 0.43 \pm 0.11$	0.496 ± 0.025	1.90 ± 0.87
195.5	$0.45 \pm 0.22 \pm 0.06$	0.531 ± 0.027	0.85 ± 0.41
199.5	$0.82 \pm 0.24 \pm 0.10$	0.567 ± 0.028	1.45 ± 0.42
201.6	$0.68 \pm 0.34 \pm 0.08$	0.587 ± 0.029	1.16 ± 0.58

Table 3: Measured and predicted hadronic cross sections for different centre-of-mass energies and the ratios between experiment and theory. For the ratios, only statistical errors are shown.

CM energy[GeV]	σ_{tot} $[pb]$	σ_{tot}(GRC4F) $[pb]$	Ratio
182.7	$0.61 \pm 0.26 \pm 0.06$	0.625 ± 0.032	0.98 ± 0.42
188.6	$0.45 \pm 0.14 \pm 0.04$	0.700 ± 0.034	0.64 ± 0.20
191.6	$1.31 \pm 0.47 \pm 0.11$	0.738 ± 0.037	1.78 ± 0.64
195.5	$0.65 \pm 0.24 \pm 0.06$	0.790 ± 0.040	0.82 ± 0.30
199.5	$0.99 \pm 0.25 \pm 0.10$	0.843 ± 0.042	1.17 ± 0.30
201.6	$0.75 \pm 0.35 \pm 0.08$	0.872 ± 0.044	0.86 ± 0.40

Table 4: Measured and predicted total cross sections for different centre-of-mass energies and the ratios between experiment and theory. For the ratios, only statistical errors are shown.

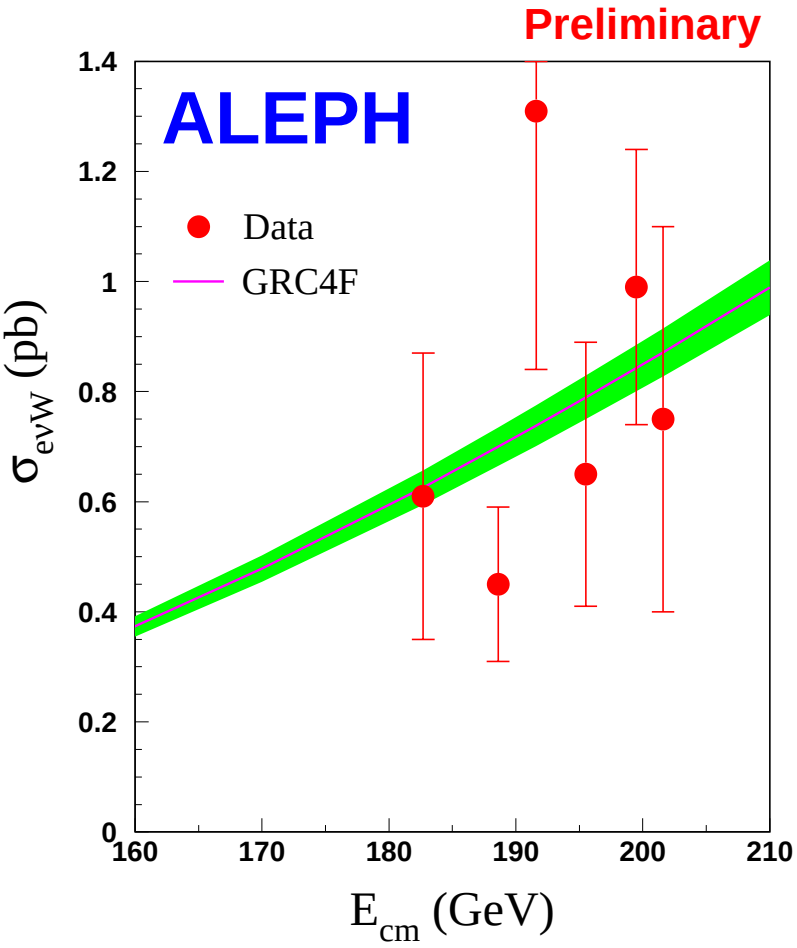

Figure 5: Measured total single W production cross section at centre-of-mass energies up to 202 GeV . The theoretical prediction with GRC4F for the signal phase space defined in equation (2) is also shown. The band represents a theoretical uncertainty of $\pm 5\%$.

which is made of a Poisson term and of a probability density function constructed from the differential cross section. For the Poisson term, N is the observed number of events and $N_\sigma(\bar{\alpha})$ is a function of the total cross section $\sigma(\bar{\alpha})$. The dependence with the couplings $\bar{\alpha}$ of the WW background is taken into account in this analysis.

The probability density function $P(O_i, \bar{\alpha})$ for an event with the kinematic configuration O_i is constructed from the differential cross section (obtained by reweighting MC events) and is normalised to unity.

In this analysis, the kinematic configuration O_i consists of one single observable. In the case of the leptonic selection, a natural choice is to use the transverse momentum of the lepton. For the hadronic selection, three different observables have been studied: $\mathrm{P_{t_W}}$, $|\cos(\theta_\mathrm{W})|$ and $|\Delta\cos(\theta_{jj})|$.

In order to choose the best kinematical variable, 200 pseudo experiments were performed (at 189 GeV) from which 95% C.L. limits on $\Delta\kappa_\gamma$ and λ_γ were extracted. The conclusion of this study is that the kinematic information for the tau channel does not improve the expected limit and that the best variable for the hadronic channel is the transverse momentum distribution. These distributions are shown in Fig.6 and Fig.7.

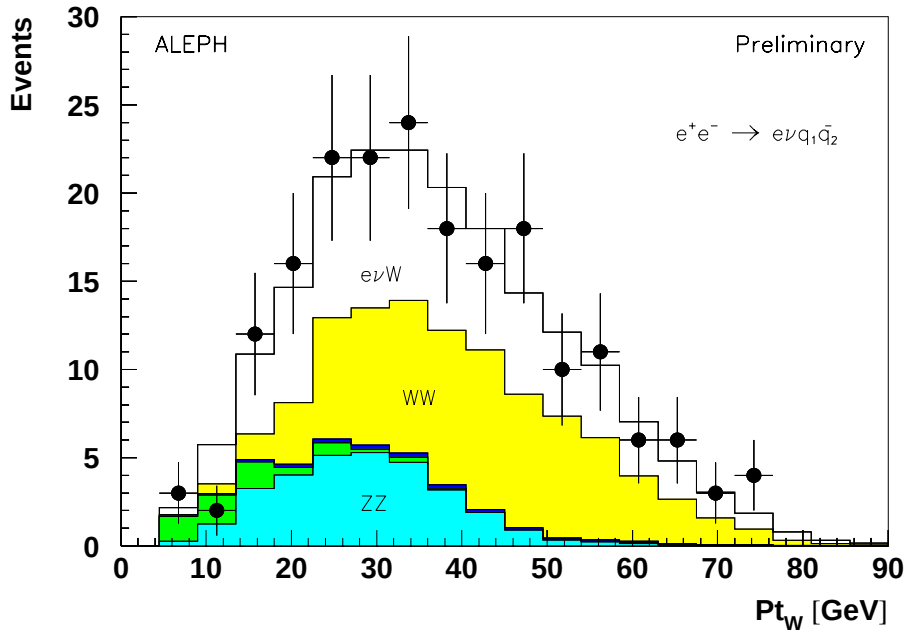

Figure 6: Comparison between distributions from the simulation (histogram) and the data (point) for the selected sample of $183 - 202$ GeV data, as function of the transverse momentum of the W. The displayed histograms represent from top to bottom the eνW, WW, various other processes, q$\bar{\mathrm{q}}$ and ZZ contributions, respectively.

6 Results

The selected single W candidates can be used to set limits on the TGCs. While the single W process is sensitive to the WWγ coupling, and in particular to κ_γ [1], the W pair production which is the main background in the hadronic decay mode is also taken into

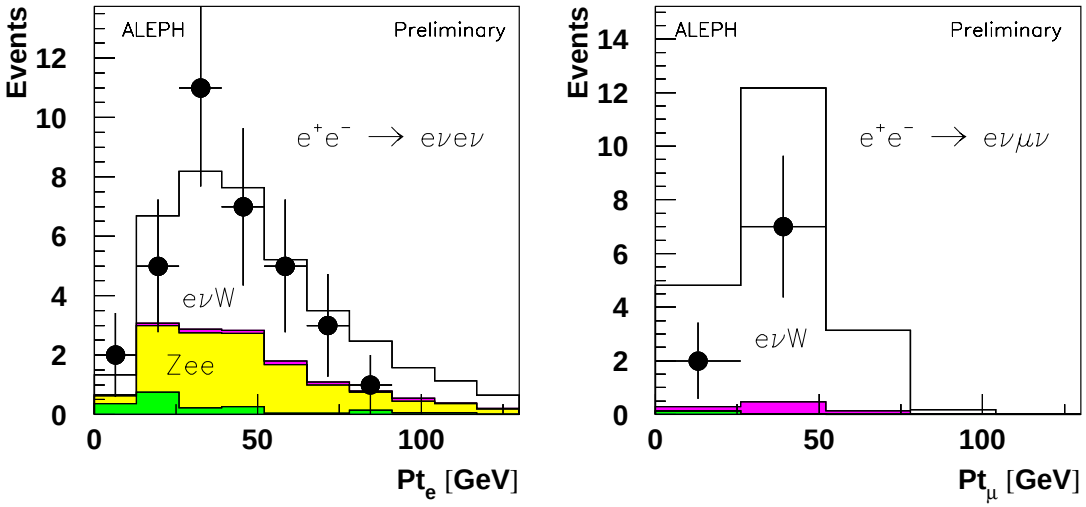

Figure 7: Comparison between distributions from the simulation (histogram) and the data (point) for the selected sample of $183 - 202\,\mathrm{GeV}$ data, as function of the transverse momentum of the lepton. The displayed histograms represent from top to bottom the $4f$ (with Zee and eνW processes shown explicitly), and $2f + \gamma\gamma$ contributions, respectively.

account in the fitting procedure. The production of W-pair depends on both the WWγ and WWZ vertices and the $SU(2)_L \times U(1)_Y$ constraints, $\Delta g_1^Z = \Delta\kappa_Z + \Delta\kappa_\gamma \tan^2\theta_W$ and $\lambda_Z = \lambda_\gamma$, have been explicitly assumed.

In this analysis, we adopt the notation of the TGCs defined in [16], that is $g_1^\gamma \equiv 1, g_1^Z, \Delta\kappa_\gamma \equiv (\kappa_\gamma - 1), \Delta\kappa_Z \equiv (\kappa_Z - 1), \lambda_\gamma, \lambda_Z$; with Standard Model values of $g_1^Z = \kappa_\gamma = \kappa_Z = 1$ and $\lambda_\gamma = \lambda_Z = 0$.

Three different unbinned maximum log-likelihood fits are performed. The first two are made assuming a Standard Model value for λ_γ and $\Delta\kappa_\gamma$ respectively while fitting respectively $\Delta\kappa_\gamma$ and λ_γ. The resulting χ^2 curves are shown in Fig. 8a and Fig. 8b.

The 95% C.L. obtained for these couplings is

$$-0.54 < \Delta\kappa_\gamma < 0.15 (\lambda_\gamma = 0)$$

and

$$-0.57 < \lambda_\gamma < 0.44 (\Delta\kappa_\gamma = 0),$$

where systematic uncertainties have been taken into account as described in section 3. For the combined likelihood, the systematic error is assumed to be 100% correlated.

A third fit is performed with both $\Delta\kappa_\gamma$ and λ_γ as free parameters. The resulting two dimensional 95% C.L. contour is shown in Fig. 9.

The systematic uncertainties on the contours are incorporated in the log L functions by convoluting the one-parameter systematic errors assuming parabolic behaviour of the systematic errors around the fitted TGC value.

7 Conclusion

Single W production is studied with data recorded with the ALEPH detector at centre-of-mass energies up to 202 GeV. The leptonic and hadronic cross sections are in good agreement with the Standard Model expectations.

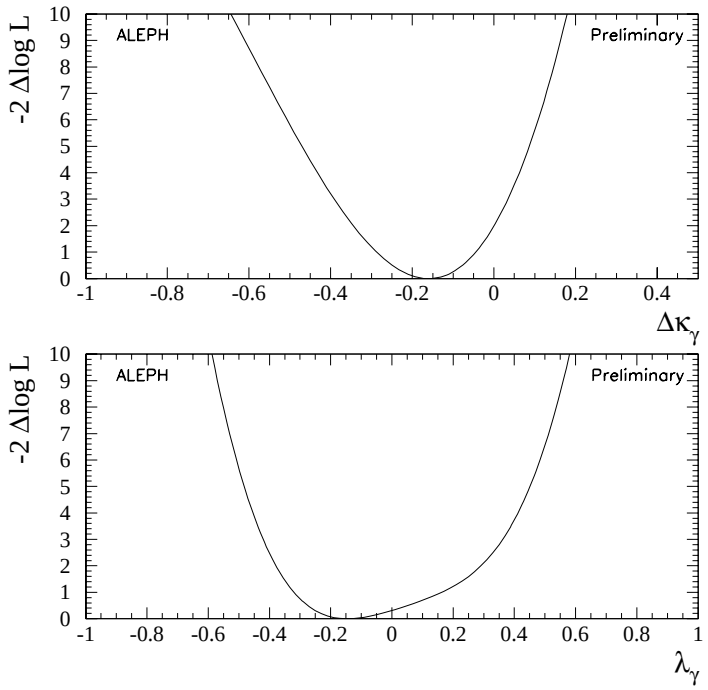

Figure 8: χ^2 curves as a function of a) $\Delta\kappa_\gamma(\lambda_\gamma = 0)$ and b) $\lambda_\gamma(\Delta\kappa_\gamma = 0)$ for $183-202\,\mathrm{GeV}$ data. The experimental systematic errors and the uncertainty of the theoretical prediction are not included in these curves.

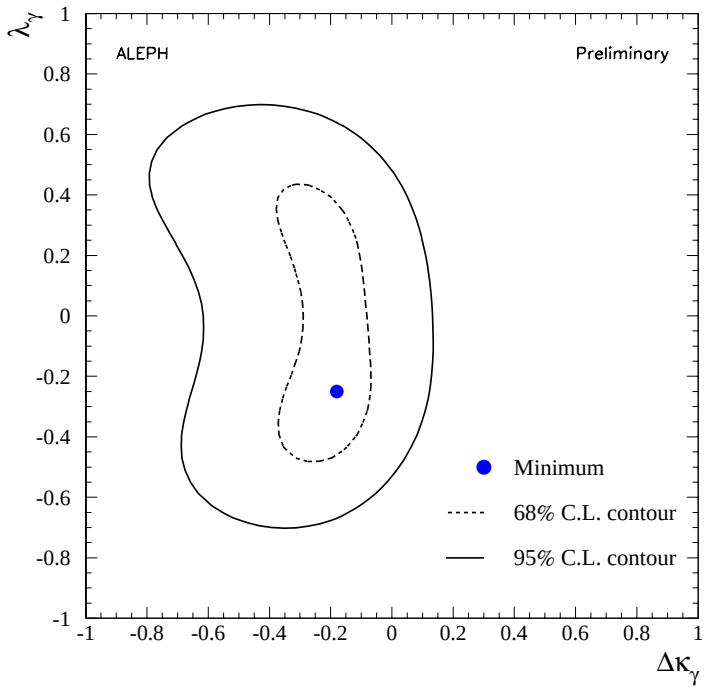

Figure 9: The contour curves for 68% C.L. and 95% C.L. in the parameter space $\Delta\kappa_\gamma - \lambda_\gamma$ for $183 - 202\,\mathrm{GeV}$ data. The systematic errors are included in these curves.

In order to illustrate the good agreement between the measurements and the Standard Model expectations, the average ratio between the total measured single W cross section and the Standard Model expectation is determined:

$$\left\langle \frac{\sigma_{e\nu W}^{\mathrm{ALEPH}}}{\sigma_{e\nu W}^{\mathrm{GRC4F}}} \right\rangle = 0.87 \pm 0.13(stat.) \pm 0.09(syst.) \pm 0.05(theory).$$

Performing an unbinned maximum log-likelihood fit, new 95% C.L. limits on TGC's are found to be $-0.54 < \Delta\kappa_\gamma < 0.15(\lambda_\gamma = 0)$ and $-0.57 < \lambda_\gamma < 0.44(\Delta\kappa_\gamma = 0)$.

Acknowledgements

We wish to congratulate the accelerator division at CERN for the successful operation of LEP in 1999. We are grateful to the engineers and technicians in our institutions for their contribution to the successful operation of the ALEPH detector. Those of us from non-member countries thank CERN for its hospitality.

References

[1] T. Tsukamoto and Y. Kurihara, Phys. Lett. **B389** (1996) 162.

[2] ALEPH Collaboration, *A Study of Single* W *Production in* e^+e^- *Collisions at* $\sqrt{s}$ *=161-183 GeV*, Phys. Lett. **B462** (1999) 389.

[3] ALEPH Collaboration, *Single* W *Production at Energies up to* $\sqrt{s} = 189\,\mathrm{GeV}$ *and Search for Monojet Events*, ALEPH/99-052, EPS-HEP99.

[4] ALEPH Collaboration, *Single* W *Production at Energies up to* $\sqrt{s} = 202\,\mathrm{GeV}$, ALEPH/00-022, Moriond2000.

[5] ALEPH Collaboration, *ALEPH: A Detector for Electron-Positron Annihilations at LEP*, Nucl. Instr. Meth. **A 294** (1990) 121.

[6] ALEPH Collaboration, *Performance of the ALEPH Detector at LEP*, Nucl. Instr. Meth. **A 360** (1995) 481.

[7] J. Schwindling, B. Mansoulie, and O. Couet, MLPFIT package (version 1.40) interfaced with PAW.

[8] J. Fujimoto *et al.*, Comp. Phys. Comm. **100** (1997) 128.

[9] E. Barberrio *et al.*, Comp. Phys. Comm. **66** (1991) 115, **79** (1994) 291.

[10] S. Jadach *et al.*, Comp. Phys. Comm. **70** (1992) 69, **76** (1993) 361.

[11] H. Anlauf *et al.*, Comp. Phys. Comm. **79** (1994) 466.

[12] S. Jadach, B.F.L. Ward, and Z. Wąs, Comp. Phys. Comm. **79** (1994) 503.

[13] T. Sjöstrand, Comp. Phys. Comm. **82** (1994) 74; *ibid.*, CERN-TH 7112/93 (1993, revised August 1994).

[14] M. Skrzypek, S. Jadach, W. Placzek and Z. Wąs, Comp. Phys. Comm. **94** (1996) 216.

[15] J.A.M. Vermaseren, Proceedings of the IVth International Workshop on Gamma Gamma Interactions, edited by G. Cochard and P. Kessler, Springer Verlag (1980), p.35; ALEPH Collaboration, Phys. Lett. **B313** (1993) 509.

[16] K. Hagiwara, K. Hikasa, R.D. Peccei and D. Zeppenfeld, Nucl. Phys. **B282** (1987) 253; K. Gaemers and G. Gounaris, Z. Phys. **C1** (1979) 259.